

NRC Publications Archive Archives des publications du CNRC

Chirp modulation stimulated Raman scattering microscopy Pegoraro, Adrian F.; Stolow, Albert

This publication could be one of several versions: author's original, accepted manuscript or the publisher's version. /
La version de cette publication peut être l'une des suivantes : la version prépublication de l'auteur, la version
acceptée du manuscrit ou la version de l'éditeur.

For the publisher's version, please access the DOI link below. / Pour consulter la version de l'éditeur, utilisez le lien
DOI ci-dessous.

Publisher's version / Version de l'éditeur:

<https://doi.org/10.1364/OE.531274>

Optics Express, 32, 18, pp. 31297-31310, 2024-08-13

NRC Publications Archive Record / Notice des Archives des publications du CNRC :

<https://nrc-publications.canada.ca/eng/view/object/?id=c8e228ff-a82b-4d07-8d56-2767f161e633>

<https://publications-cnrc.canada.ca/fra/voir/objet/?id=c8e228ff-a82b-4d07-8d56-2767f161e633>

Access and use of this website and the material on it are subject to the Terms and Conditions set forth at

<https://nrc-publications.canada.ca/eng/copyright>

READ THESE TERMS AND CONDITIONS CAREFULLY BEFORE USING THIS WEBSITE.

L'accès à ce site Web et l'utilisation de son contenu sont assujettis aux conditions présentées dans le site

<https://publications-cnrc.canada.ca/fra/droits>

LISEZ CES CONDITIONS ATTENTIVEMENT AVANT D'UTILISER CE SITE WEB.

Questions? Contact the NRC Publications Archive team at

PublicationsArchive-ArchivesPublications@nrc-cnrc.gc.ca. If you wish to email the authors directly, please see the
first page of the publication for their contact information.

Vous avez des questions? Nous pouvons vous aider. Pour communiquer directement avec un auteur, consultez la
première page de la revue dans laquelle son article a été publié afin de trouver ses coordonnées. Si vous n'arrivez
pas à les repérer, communiquez avec nous à PublicationsArchive-ArchivesPublications@nrc-cnrc.gc.ca.



Chirp modulation stimulated Raman scattering microscopy

ADRIAN F. PEGORARO^{1,2,6}  AND ALBERT STOLOW^{2,3,4,5,7}

¹*Metrology Research Centre, National Research Council of Canada, 100 Sussex Drive, Ottawa, ON, K1A 0R6, Canada*

²*Department of Physics, University of Ottawa, Ottawa ON, K1N 6N5, Canada*

³*Department of Chemistry, University of Ottawa, Ottawa ON, K1N 6N5, Canada*

⁴*Max-Planck-Ottawa Centre for Extreme and Quantum Photonics, Ottawa ON, K1N 6N5, Canada*

⁵*Quantum and Nanotechnologies Research Centre, National Research Council of Canada, 100 Sussex Drive, Ottawa, ON, K1A 0R6, Canada*

⁶*adrian.pegoraro@nrc-cnrc.gc.ca*

⁷*astolow@uottawa.ca*

Abstract: Coherent Raman microscopy, a rapid, chemical-specific, label-free imaging method, can be plagued by non-Raman background signals. Existing modulation schemes mitigate these but none remove all background signals. Here we demonstrate what we believe to be a novel scheme, chirp modulation stimulated Raman scattering (CM-SRS), based upon modulating uniquely the relative sign of the quadratic phase (linear chirp) of the input lasers. CM-SRS removes all non-Raman signals and is linear in both Raman oscillator strength and concentration. We demonstrate that CM-SRS is highly sensitive, quantitative, and background-free via imaging of traditionally challenging samples and the small molecule pharmacokinetics of single living cells.

©2024 Optica Publishing Group under the terms of the [Optica Open Access Publishing Agreement](#)

1. Introduction

Optical phase control of coherent broadband pulses, which plays no role in linear optics, is important in nonlinear optical spectroscopy and microscopy. This is particularly so in Coherent Raman Microscopies (CRMs), where control over optical phase is used to enhance chemical specificity, sensitivity and image contrast [1–4]. CRM, comprising a set of nonlinear stimulated Raman techniques typically requiring as input two ultrashort laser pulses (Pump and Stokes), is valued for its rapid imaging speed and potential for increased sensitivity [5–9] as compared with conventional spontaneous Raman scattering. While CRM avoids some background signals which plague spontaneous Raman microscopy, it is not inherently background free. Rather, CRM is a third-order nonlinear optical process which competes with a range of nonlinear optical processes generating background signals. These non-Raman processes, which include excited state absorption (ESA), thermal lensing (TL), two-photon absorption (TPA), cross-phase modulation (XPM) and four-wave mixing (FWM), limit CRM imaging in broad ranges of materials including nanostructures [10,11], minerals [12,13], plants [14,15] and pigments [16,17]. In favourable cases, these non-Raman signals may identify specific species [10,17–19] but this requires instrument and species-specific calibration. More generally, there has been a global effort to minimize non-Raman backgrounds in CRM, often using well-known linear optical modulation transfer schemes developed for telecommunications and optical spectroscopy [20–22]. Canonical examples include amplitude modulation (AM) [23], polarization modulation (PM) [12] and frequency modulation (FM) [15,24–27]. Unfortunately, none of the existing schemes simultaneously remove all non-Raman background terms, ultimately limiting the sensitivity and contrast of CRM and, therefore, its extension to even broader fields of research. Here we propose

and demonstrate Chirp Modulation Stimulated Raman Scattering (CM-SRS), a nonlinear optical modulation scheme which completely removes all non-Raman background signals in CRM.

Unlike traditional linear optical modulation, we take advantage of the control over nonlinear optical processes afforded by the optical phase of coherent broadband pulses [1,28,29]. The optical phase is commonly expressed as a series expansion about the central carrier frequency, with the linear term being the frequency, the quadratic term being the chirp, etc. The well-known frequency modulation (FM) technique is an example of the modulation of the linear phase (i.e. frequency). An example of quadratic phase control in CRM is termed spectral focussing wherein the input Pump and Stokes pulses are ‘co-chirped’, meaning that they have identical sign and magnitude of quadratic phase (chirp). In spectral focussing CRM, the chirp magnitude sets the instantaneous Pump-Stokes frequency difference and, hence, the effective Raman spectral resolution [30–33]. Conveniently, Raman spectral scanning is achieved here simply by changing the time delay between the two pulses. Spectral focussing operates using fixed higher-order phase terms and, therefore, is not a modulation technique which removes background signals. Rather, signal recovery in spectral focusing CRM has, to date, been based on traditional linear optical modulation techniques [12,32,34]. Central to the present work, we note that signal recovery schemes in nonlinear optical spectroscopies and microscopies, including CRM, can also be based on the modulation of higher order phase terms. However, nonlinear optical processes also depend strongly on intensity [35] and, therefore, care must be taken to ensure that any applied modulations of higher-order phases do not introduce undesired intensity modulations. This can be achieved by maintaining constant pulse duration during the applied modulation. This, in turn, is achieved by constraining the higher order phase modulations to even/odd symmetry about the central carrier frequency. We exemplify this novel approach to signal recovery in nonlinear optical spectroscopy/microscopy by applying a rapid modulation to the sign - but not the magnitude - of the quadratic phase (linear chirp) of an optical pulse: maintaining constant magnitude of the quadratic phase ensures constant pulse duration and, therefore, intensity.

Under chirp modulation, two-photon resonant signals may be modulated, including both electronic and Raman resonances. Signals from sharp two-photon resonances, whether at the sum (i.e. TPA) or difference (i.e. SRS) frequency, will be significantly modulated whereas signals from broad resonances will not. More precisely, two-photon resonances spectrally narrower than the laser bandwidth will produce modulated signals, whereas resonances broader than this will not. For many samples of interest, this means that the Raman resonant signal will be modulated whereas non-Raman CRM background signals (TL, XPM, TPA, ESA) will not, enabling their removal via modulation transfer with lock-in detection. We term this scheme Chirp Modulation SRS (CM-SRS). While illustrated for SRS, we note that chirp modulation is applicable to other types of CRM including coherent anti-Stokes Raman scattering (CARS) and coherent Stokes Raman scattering (CSRS) [26], as well as any other nonlinear optical micro/spectroscopies, such as sum-frequency generation, where control over higher order optical phases is useful. We experimentally demonstrate that CM-SRS completely removes all non-Raman background signals, leading to significantly enhanced Raman sensitivity and contrast, even in complex heterogenous, strongly absorbing materials. We anticipate that CM-SRS will broaden the applications of CRM to new classes of challenging samples and materials.

2. Materials and methods

CM-SRS is based upon modification of a spectral focusing AM-SRS setup described previously [13]. The current setup is shown in Fig. 1. Briefly, a dual output Insight DS + laser (Spectra-Physics, USA) produced two synchronized outputs at 80 MHz repetition rate. One (here the SRS Pump beam, blue) is tunable from 680-1300 nm, with a transform-limited pulse duration of approximately 120 fs across this tuning range. The second output (the SRS Stokes beam, red) was centered at a fixed wavelength of 1040 nm and has a transform-limited pulse duration

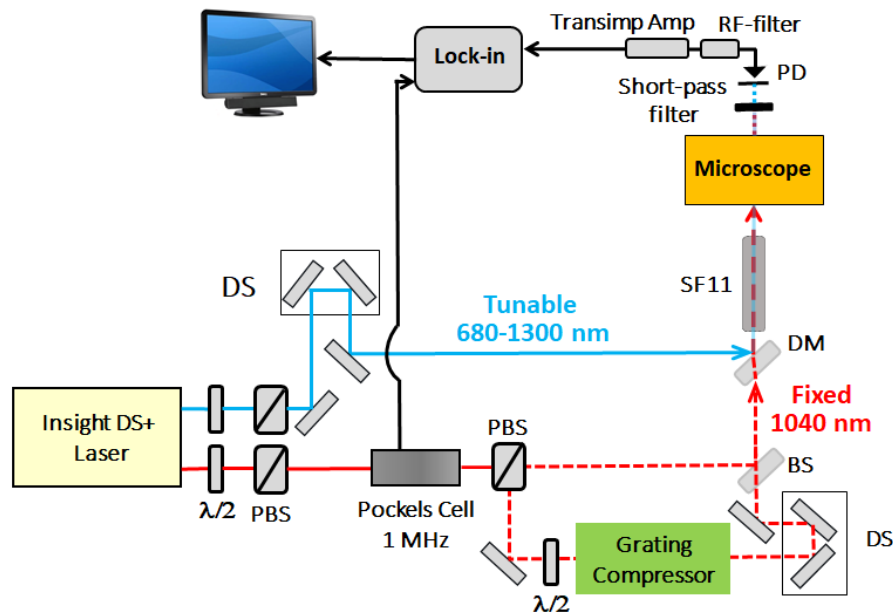


Fig. 1. CM-SRS setup. $\lambda/2$ is a half-wave plate. PBS is polarized beam splitter. BS is a beam splitter. DM is a dichroic mirror. DS is the delay stage used for scanning the time delay (Raman shift in spectral focusing) SF11 is 60 cm of AR coated glass. PD is a photodiode. For details, see the text.

of 220 fs. The Stokes beam was used to generate the requisite co-chirped and contra-chirped configurations, described below. The tunable Pump output was passed through a half-wave plate ($\lambda/2$) and polarizing beam splitter (PBS) to control the average power, before being sent to a variable delay stage (DS, for scanning of the Raman spectrum in spectral focusing) and then to a dichroic mirror (DM) recombiner (Pump + Stokes). The fixed 1040 nm Stokes output was sent through a Pockels cell (350-160, Conoptics, USA) modulated at 1 MHz, the driving waveform for which was provided by a function generator (DS345, Stanford Research Systems, USA). For AM-SRS implementations, following a PBS, the rejected output (vertical dashed red line) was blocked and the transmitted output (horizontal dashed red line) was sent to the DM recombiner. The combined Pump and Stokes beams were sent through 60 cm of SF11 glass, thus providing the co-chirped configuration. To ensure that the magnitudes of the linear chirps of the three input beams (pump, co-chirped Stokes, contra-chirped Stokes) are well matched, we utilized the internal, tunable dispersion compensation provided by the Insight laser to achieve chirp matching at the focus of the microscope. For CM-SRS implementations, the rejected output, used to generate the contra-chirped beam, was sent through a $\lambda/2$ plate to rotate the beam to the same polarization state as the co-chirped output, and then to a grating compressor, followed by a delay stage to accurately synchronize the two 1040 nm beams. The co- and contra-chirped Stokes beams were recombined using a 50:50 beam splitter (BS) before being sent to the DM recombiner and the 60 cm SF11 glass. Note that the grating compressor was adjusted so that despite the 60 cm of glass the correct contra-chirped configuration (see Fig. 2(a)) was achieved at the microscope focus. Therefore, by blocking or unblocking the CM-SRS contra-chirped arm, one can seamlessly switch between AM- and CM-SRS. Importantly: for CM-SRS measurements, the modulation between the co- and contra-chirped beams is set by the Pockels cell at 1 MHz rate in the current implementation. The home-built microscope used galvo mirrors (GVSM002-US, Thorlabs, USA) connected to a microscope frame (Olympus IX-71). Measurements of DMSO

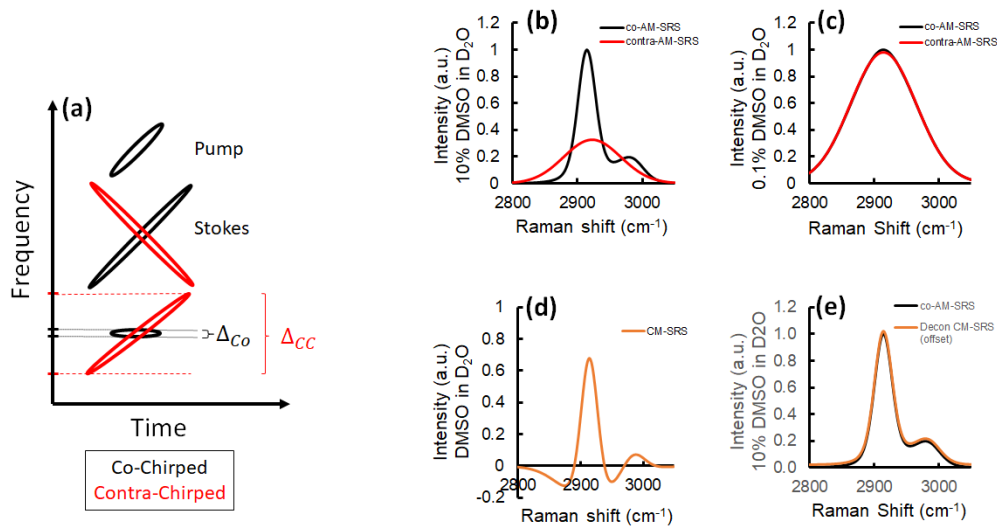


Fig. 2. Comparison of AM-SRS and CM-SRS (a) Using a frequency-time plot, it is possible to visualize how the Raman resolution is changed in AM-SRS between the co-chirped case (black shapes) compared to the contra-chirped case (red shapes). For co-chirped AM-SRS, Δ_{Co} becomes smaller as the chirp increases whereas for contra-chirped AM-SRS Δ_{CC} remains constant as the chirp magnitude increases. (b) Numerical simulation of co- (black line) and contra-chirped (red line) AM-SRS of DMSO in D₂O in the strong (i.e. background-free) Raman signal regime. (c) Numerical simulation of co- (black line) and contra-chirped (red line) AM-SRS in the weak (i.e. background dominant) Raman signal regime. (d) Numerical simulation of CM-SRS; the shape of the spectral response is identical for both the strong and weak Raman signal regimes. (e) Comparison of the deconvolved CM-SRS response (orange line) and the background-free co-chirped AM-SRS signal from the strong Raman regime (black line). The linear deconvolution procedure is detailed in the text. The spectra are numerically offset here in order to permit comparison.

spectra and HepG2 cells used a 60x, 1.2 NA water objective (UPlanSapo, 60x, 1.2 NA, Olympus, Japan) whereas measurements of sweet potato and pine stem samples used a 20x, 0.75 NA air objective (UPlanSapo, 20x, NA 0.75, Olympus, Japan). In all cases, forward propagating light was collected using an objective lens (LUMPlanFI/IR, 40x, NA 0.8 water immersion, Olympus, Japan). Collected light was filtered (BrightLine 850/310, Semrock, USA and 1064-71 NF, Iridian, Canada) to remove the Stokes light before being sent to a photodiode (PD, FDS10X10, Thorlabs, USA) operating under reverse bias. The photodiode signal was filtered using 1 MHz bandpass RF filter (#3128, KR Electronics, USA) before being amplified by a transimpedance amplifier (DHCPA-100 Femto Messtechnik, GmbH, Germany). The output of the amplifier was sent to a lock-in amplifier (UHFLI, Zurich Instruments) which was referenced to the Pockels cell drive signal. Typically, a 20 μ s time constant was used. All data collection and drive of the galvanometer mirrors were synchronized using ScanImage [36]. For all measurements, the power in each 1040 nm arm of the AM and CM-SRS was 50 mW before the microscope. For the DMSO measurements, the tunable arm was set to 796 nm central wavelength with an average power of 100 mW before the microscope. For the sweet potato measurements, the tunable arm was set to 898, 912, and 929 nm central wavelengths with 50 mW average power. For measurements of HepG2 cells, the tunable beam was set to a central wavelength of 800 nm with average power of 50 mW for measurements around a Raman shift of 2850 cm^{-1} , whereas a central wavelength of 844 nm with an average power of 100 mW was used for measurements around a Raman shift of

2230 cm^{-1} . To acquire Raman spectra, the time delay between the pump and Stokes beams was scanned so as to vary the instantaneous frequency difference between the lasers.

3. Results and discussion

3.1. Theory and simulation

In spectral focusing CRM, femtosecond Pump and Stokes input pulses are co-chirped with both the sign and magnitude of their quadratic phase terms set equal so that their instantaneous frequency difference remains constant across their spectral width: the chirp magnitude determines the effective Raman spectral resolution. A frequency-time representation of co-chirped spectral focusing CRM is shown (black) in Fig. 2(a). The effective Raman spectral resolution, Δ_{Co} , is the projection (dashed black lines) onto the frequency axis. As long as the chirps are held equal, by using adaptive optics to correct for higher order phase terms [37], the achievable Raman spectral resolution increases with chirp magnitude and can be optimized for a given sample [31]. There is, however, a “worst” possible Raman resolution in spectral focusing: transform-limited pulses yield an effective resolution determined by the convolution of the broadband input pulse spectra. Interestingly, this same “worst” resolution is achieved if the two input beams have the same magnitude but opposite signs of quadratic phase (linear chirp), as illustrated in red in Fig. 2(a), with the effective spectral resolution, Δ_{CC} indicated by the dashed red lines. We term this scheme contra-chirped, distinguishing it from the co-chirped case. In CM-SRS, we rapidly modulate between these two schemes, where the sign but not the magnitude of the relative chirp is changed, causing the effective Raman spectral resolution to modulate between Δ_{Co} and Δ_{CC} while keeping all other laser parameters invariant. Non-Raman background terms, using standard spectrally integrated detection, are insensitive to the sign of the chirp and are therefore subtracted, resulting in background-free Raman-resonant signals.

An advantage of SRS is its linear scaling with concentration which, absenting non-Raman background signals, allows for quantitative imaging. To illustrate this for CM-SRS, we numerically modeled [31,38] spectral focusing AM-SRS of dimethyl sulfoxide (DMSO) in the CH region ($\sim 2900 \text{ cm}^{-1}$) and included a weak non-Raman background chosen to simulate XPM, often a major contributor to background in SRS microscopy. Here, we modeled the process using wavelength tuning as opposed to delay-tuning used in spectral focusing and scaled the pump intensity to account for the changing overlap experienced in our experimental implementation of spectral focusing. We set the co-chirped spectral resolution to $\sim 20 \text{ cm}^{-1}$, the contra-chirped to $\sim 120 \text{ cm}^{-1}$. Guided by experiment [12], we investigated two regimes: (i) strong Raman signals corresponding to 10% (v/v) DMSO in D_2O ; (ii) weak Raman signals corresponding to 0.1% (v/v) DMSO in D_2O . In the strong signal case, co-chirped AM-SRS yields a high-resolution spectrum shown by the black curve in Fig. 2(b), essentially the spontaneous Raman spectrum of DMSO. Contra-chirped SRS provides poor spectral resolution and a largely featureless spectrum, the red curve in Fig. 2(b). In the weak signal case, Fig. 2(c), both the co-chirped (black) and contra-chirped (red) AM-SRS spectra are largely featureless, due to the dominant non-Raman background obscuring the Raman spectrum. The CM-SRS spectrum, Fig. 2(d) (orange), is the difference between the co- and contra-chirped spectra: note that both the strong and weak signal CM-SRS spectra are identical up to a linear concentration-dependent scale factor and therefore we show only one case here.

Importantly, the CM-SRS spectrum yields the same chemical-specific information as would the completely background-free AM-SRS Raman spectrum. We examined the unusual CM-SRS spectral line shape, Fig. 2(d), via an analytic expression for the generated third order polarization, assuming Lorentzian Raman resonance line shapes and Gaussian laser pulse spectra. Using a standard formulation [31,38], the generated 3rd order polarization, $P^{(3)}$ can be shown (see Supplement 1) to be given by the convolution of a Lorentzian Raman resonance with an effective (i.e. chirp dependent) Gaussian excitation (i.e. Pump-Stokes difference frequency) spectrum:

this convolution is a Voigt lineshape. For the co-chirped case, the Gaussian excitation has an effective spectral width given by:

$$\Delta_{Co} = \frac{\Delta_{laser}\sqrt{2}}{\sqrt{1+a^2}} \quad (1)$$

whereas for the contra-chirped case, excitation Gaussian effective spectral width is independent of the chirp magnitude:

$$\Delta_{CC} = \Delta_{laser}\sqrt{2} \quad (2)$$

where Δ_{laser} is the spectral width of both the pump and Stokes and a is the effective chirp parameter. As expected, the effective spectral resolution is superior for the co-chirped case ($\Delta_{Co} \leq \Delta_{CC}$) and the contra-chirped spectral resolution is the same for all chirp magnitudes a . Importantly, the non-Raman terms are independent of the sign of the chirp and thus are effectively removed by CM-SRS, as shown in [Supplement 1](#). To elucidate this point and to clarify the linear deconvolution procedure, we present below a simplified discussion of CM-SRS signal generation. In standard AM-SRS, the co-chirped spectrum is given by:

$$S_{Co}(\omega) = G_{Co} * S_{Raman}(\omega) + B(\omega) = S_{AM}(\omega) \quad (3)$$

where $S_{AM}(\omega)$ is the usual AM-SRS spectrum, G_{Co} is a Gaussian excitation spectrum having a co-chirp dependent spectral width given by Eq. (1), $S_{Raman}(\omega)$ is the spontaneous Raman spectrum and $B(\omega)$ is the sum of all non-Raman background signals, assumed to be independent of the sign of the chirp. In the strong Raman signal regime, the background $B(\omega)$ may become negligible and, therefore, the strong signal AM-SRS spectrum should be linearly proportional to the spontaneous Raman spectrum. For the contra-chirped case, we have:

$$S_{CC}(\omega) = G_{CC} * S_{Raman}(\omega) + B(\omega) \quad (4)$$

where $S_{CC}(\omega)$ is the contra-chirped AM-SRS spectrum, G_{CC} is a Gaussian excitation with a spectral width given by Eq. (2) and is independent of the chirp magnitude. The non-Raman $B(\omega)$ terms are as in Eq. (3). In CM-SRS, we dynamically subtract of Eq. (4) from (3) to generate:

$$S_{CM}(\omega) = (G_{Co} - G_{CC}) * S_{Raman}(\omega) \quad (5)$$

where $S_{CM}(\omega)$ is the CM-SRS spectrum. We note several important aspects of Eq. (5). First, the CM-SRS spectrum is linearly proportional to the spontaneous Raman spectrum and thus can be used directly to quantitatively measure concentrations without the need for deconvolution. Furthermore, just as is the case for AM-SRS, there is no coherent interference between Raman resonances (see [Supplement 1](#), Fig. S1). Second, the CM-SRS spectrum has no background term, independent of the Raman signal strength. Third, for an isolated Raman resonance, the lineshape is expected to exhibit a central peak with symmetric negative signals on either side, as in Fig. 2(d). Fourth, if a background-free AM-SRS spectrum can be recorded (for example, in the strong Raman signal regime), then CM-SRS permits recovery of the background-free AM-SRS spectrum under all experimental conditions. This, in turn, requires use of the CM-SRS deconvolution kernel, obtained from the instrument response function *IRF*. Assuming that the background term can be effectively neglected in the strong Raman signal regime, the AM-SRS spectrum becomes:

$$S_{AMStrong}(\omega) = G_{Co} * S_{Raman}(\omega) \quad (6)$$

then

$$F\{S_{Raman}\} = \frac{F\{S_{AMStrong}(\omega)\}}{F\{G_{Co}\}} \quad (7)$$

where $F\{\}$ is the Fourier transform. Upon substitution of Eq. (7) into the Fourier transform of Eq. (5), we obtain:

$$F\{S_{AMStrong}(\omega)\} = F\{S_{CM}(\omega)\} \frac{F\{G_{Co}\}}{F\{G_{Co} - G_{Cc}\}} = F\{S_{CM}(\omega)\} F\{IRF\} \quad (8)$$

where IRF is the sample-independent instrument response function for CM-SRS. In practice, the CM-SRS spectrum should be measured on the same sample as $S_{AMStrong}(\omega)$. To illustrate this point, in Fig. 2(e) we show the deconvolved CM-SRS spectrum of Fig. 2(d) overlaid with the strong Raman signal AM-SRS spectrum (i.e. the background-free AM-SRS spectrum) of Fig. 2(b). The deconvolved CM-SRS spectrum (orange) and the strong Raman signal AM-SRS spectrum of Fig. 2(b) (black) are effectively identical, absenting noise, and are artificially offset here to distinguish them.

A few limitations of CM-SRS can also be deduced from an examination of the above equations. First, we note that the CM-SRS signal is always slightly lower than the AM-SRS signal, since the subtraction of the contra-chirped beam in CM-SRS always entails the subtraction of a small resonant component. Therefore, if the limiting concern is noise, it may be preferable to apply standard AM-SRS, since the signal-to-noise ratio will be slightly higher. However, if the limiting concern is background signals, then CM-SRS is demonstrably superior, as detailed here. Second, if the AM-SRS spectrum is recovered using deconvolution, noise and incomplete background removal are concerns, as is the case for all deconvolution procedures. Smoothing or filtering can be used to reduce noise but will result in poorer spectral resolution in the recovered spectrum; in systems for which AM-SRS measurements are difficult, this is likely an acceptable compromise. Third, CM-SRS assumes that the background signal is not phase coherent with the desired signal. While valid for SRS imaging, this assumption fails if the CM approach is applied to CARS microscopy and full background subtraction cannot be achieved (see [Supplement 1](#), Fig. S2 for further discussion).

Finally, the above analysis provides a framework for discussing the effects of spectral width of the Raman-resonant and non-Raman background terms on the recovered signals. We have made two assumptions: 1) the Raman resonance is narrow relative to the laser bandwidth; 2) the background signals are not very strongly chromatic. Given we use femtosecond lasers in CM-SRS, the first assumption holds for many Raman modes of interest but not all (water, for example). When this assumption is violated, the relative difference between the co- and contra-chirped AM-SRS contributions becomes increasingly small and the CM-SRS signal strength concomitantly decreases. The retrieved Raman lineshapes, however, remain unaffected, albeit with reduced signal-to-noise ratios. The second assumption is a significant relaxation of a requirement for FM-SRS: in FM-SRS it is assumed that the non-Raman background is achromatic over the modulation range of the center wavelength of the lasers of interest (100s-1000 cm^{-1}), whereas in CM-SRS we require that the background be achromatic only over the narrow bandwidth of the excitation laser ($\sim 80 \text{ cm}^{-1}$), a much relaxed constraint.

3.2. Experimental results

We experimentally demonstrated CM-SRS using a modified spectral focusing AM-SRS microscope wherein the instantaneous frequency difference follows the time delay between the input lasers, mapping linearly onto Raman frequency. Conventionally, scanning the time delay between the input pulses measures their cross-correlation: therefore, the non-Raman signals in spectral focusing AM-SRS will not appear flat but rather will follow the known spectral cross correlation between the two input pulses. In CM-SRS, where all non-Raman signals are dynamically subtracted, this is not a concern. In the simulations above we assumed, for calculational simplicity, that the central (difference) frequency was tuned rather than scanning the time delay between the input pulses. However, in spectral focusing SRS, the time delay

scan is equivalent to tuning the instantaneous difference frequency plus a phase shift. Since the latter does not modify the CM-SRS spectral response, this validates the simulations. To further verify that this subtraction of non-Raman background can be achieved experimentally, we measured the cross-correlation of the co- and contra-chirped Stokes beams with the pump using non-degenerate two-photon excited fluorescence (TPEF). We observed that the co- and contra-chirped TPEF signals are nearly identical (see [Supplement 1](#), Fig. S3), despite the lack of corrections to the higher-order (i.e. beyond quadratic) phases. Indeed, when performing a CM-SRS measurement on such a sample, the non-Raman signals were completely subtracted, resulting in a null signal as expected.

To directly compare experiment with simulation, we measured the CM-SRS spectrum of DMSO in D₂O in the C-H stretch region as a function of concentration. In Fig. 3, we show the strong (10% v/v DMSO) and weak (0.1% v/v DMSO) Raman signal regimes. In the strong Raman signal regime, we separately recorded co-chirped and contra-chirped AM-SRS spectra, Fig. 3(a). Co-chirped AM-SRS (black) provides a high-resolution spectrum, whereas contra-chirped AM-SRS (red) yields a low-resolution spectrum. Based on these measurements, we estimate our co-chirped AM-SRS resolution to be $\sim 25\text{ cm}^{-1}$ and our contra-chirped AM-SRS resolution to be $\sim 80\text{ cm}^{-1}$. In Fig. 3(b), the weak Raman signal (0.1% v/v DMSO) regime, both the co-chirped (black) and contra-chirped (red) AM-SRS spectra are largely featureless being dominated by non-Raman background. In CM-SRS, we modulate at high frequency between the co- and contra-chirped case, yielding the CM-SRS spectrum in Fig. 3(c) (orange) shown for the strong signal regime. The CM-SRS spectrum is the dynamic subtraction of two AM-SRS spectra. In the strong signal regime, this is demonstrated by subtracting—post measurement—the co-chirped (black) and contra-chirped (red) spectra of Fig. 3(a). The result of this ‘static’ subtraction is shown in blue in Fig. 3(c). The SRS spectrum constructed from the difference between sequentially recorded scans (blue) is nearly identical to the CM-SRS spectrum (orange), with small differences attributed to residual low frequency noise which is removed by the high frequency modulation of CM-SRS. Similarly, as shown in Fig. 3(d) (orange), CM-SRS yields a Raman-resonant spectrum even in the weak signal regime. However, the demonstration that this is equivalent to the ‘static’ difference spectrum was not possible in the weak signal regime since the AM-SRS spectra were dominated by non-Raman processes and low-frequency noise. Importantly, we can deconvolve CM-SRS spectra to recover background-free AM-SRS Raman spectra. We obtained a deconvolution kernel in the strong Raman regime using AM-SRS and CM-SRS spectra and applied it to the weak-signal CM-SRS spectrum, yielding the retrieved spectrum in Fig. 3(d) (grey) which is equivalent to a background-free AM-SRS spectrum. To show this, we assumed, as is conventional, that co-chirped AM-SRS spectrum of Fig. 3(a) (black) is linearly proportional to concentration and can scaled down (here by a factor of 100) serving as a proxy for the spontaneous Raman spectrum in Fig. 3(d) (black). The deconvolved CM-SRS spectrum (grey) and predicted spontaneous Raman spectrum (black) very closely agree, demonstrating that CM-SRS yields spontaneous Raman spectra in even the weak signal limit. Note, while hard to discern, the second (small) peak of DMSO centered at 2993 cm^{-1} is not visible above the noise in Fig. 3(d); as such, this peak is not recovered in the deconvolved spectrum, highlighting the well-known fact that the deconvolution procedures cannot improve signal-to-noise ratios, typically somewhat worsening them.

An advantage of SRS over CARS microscopy is its linear scaling with concentration. As CM-SRS is linearly proportional to the Raman cross-section, its signals should scale linearly with concentration. We compared co-chirped AM-SRS with CM-SRS over a very wide range of DMSO concentrations (in D₂O), shown in Fig. 3(e). At high concentrations, both AM-SRS and CM-SRS scale linearly. At lower concentrations, AM-SRS becomes dominated by non-Raman backgrounds, no longer tracking sample concentration. In contrast, the CM-SRS signal varies linearly with concentration to very low values. In this proof-of-concept implementation, the

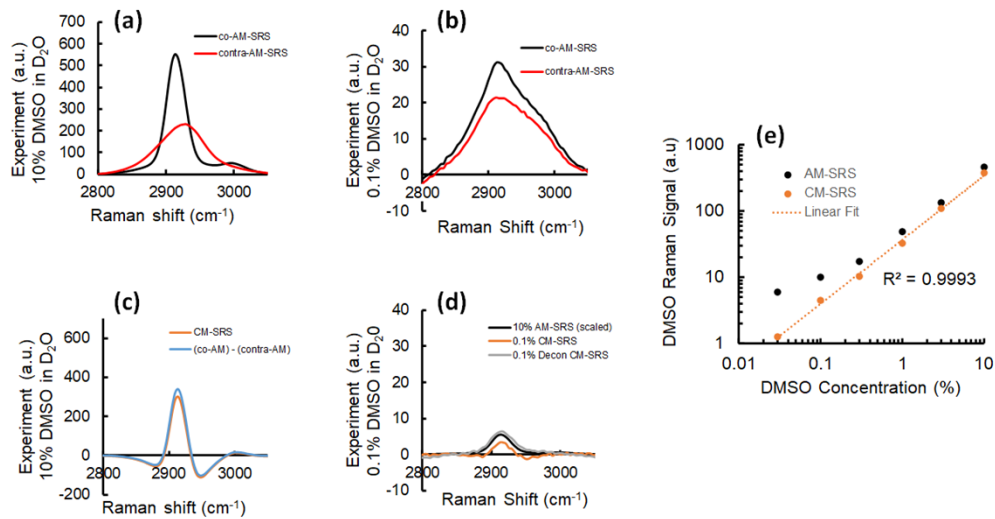


Fig. 3. Experimental demonstration of CM-SRS. In all figures, experimental signals are directly related to the measured strength of the modulation signal on the lock-in amplifier and are thus on a fixed scale. (a) Measurement of 10% (v/v) DMSO in D₂O using co- (black line) and contra-chirped (red line) AM-SRS. (b) Measurement of 0.1% (v/v) DMSO in D₂O using co- (black line) and contra-chirped (red line) AM-SRS. (c) Measurement of 10% (v/v) DMSO in D₂O using CM-SRS (orange line). As a point of comparison, the independently recorded signals in (a) were subtracted and are shown (co-AM)-(contra-AM) (blue line). (d) Measurement of 0.1% (v/v) DMSO in D₂O using CM-SRS (orange line). The deconvolution of that signal is shown as the grey line. As a point of comparison, the co-chirped AM-SRS signal from (a) is scaled by 100 and shown a black line. (e) Strength of signal on a fixed intensity scale for AM-SRS (black dots) and CM-SRS (orange dots) as a function of DMSO concentration. The orange dashed line is a linear least-squares fit to the CM-SRS data.

absolute detection limit (4.2 mM) in CM-SRS is seen here to be an order of magnitude lower than in AM-SRS, limited here by laser power and detector saturation. Thus, absolute sensitivity limits in CM-SRS should be comparable to other modulation schemes such as PM-SRS and FM-SRS which also remove cross-phase and thermal lens modulation background.

To demonstrate that CM-SRS enhances Raman contrast in complex, heterogeneous, strongly absorbing media, we imaged traditionally challenging samples: plant materials. These are generally highly colored and therefore present a great challenge to CRM, generating strong non-Raman background at all Raman shifts. We first imaged the distribution of β -carotene in plant material: its strongly chromatic nonlinear response can cause challenges for FM-SRS techniques [15]. To demonstrate the power of CM-SRS, we imaged a thin slice of sweet potato (*Ipomoea batatas*) rich in β -carotene and other phytochemicals. The Raman spectrum of β -carotene [39,40] is characterized by peaks near 1150 and 1520 cm^{-1} . Using AM-SRS, we recorded images with high spatial contrast at different Raman shifts. However, the AM-SRS image has significant background. We show in Fig. 4(a) an AM-SRS image recorded at 3 different peaks, 1150 cm^{-1} (cyan), 1520 cm^{-1} (magenta) and 2850 cm^{-1} (yellow). As can be seen, there is significant overlap in the different channels. Additionally, there are significant signals at all Raman shifts, even off resonance (see Supplement 1, Fig. S4). Thus, the apparent ‘Raman spectrum’ as measured by AM-SRS is dominated by non-Raman background which, as a function of time delay in spectral focusing AM-SRS, appears as a Gaussian spectral cross-correlation (see Supplement 1, Fig. S4). CM-SRS of the same thin section, shown in Fig. 4(b), demonstrates chemical-specific contrast and vibrationally resolved Raman spectra, permitting spatial segmentation of two different

carotenoids (magenta and cyan). Shown in yellow in Fig. 4(b) is CM-SRS in the CH-Raman region near 2850 cm^{-1} , showing the spatial distribution of starches and sugars in the sample. The segmentation-associated CM-SRS spectra of the two phytochemicals are shown in Fig. 4(c) (deconvolved Raman spectra are shown in Supplement 1, Fig. S4), thus demonstrating the chemical-specific imaging power of hyperspectral CM-SRS, even in samples with very large non-Raman background signals.

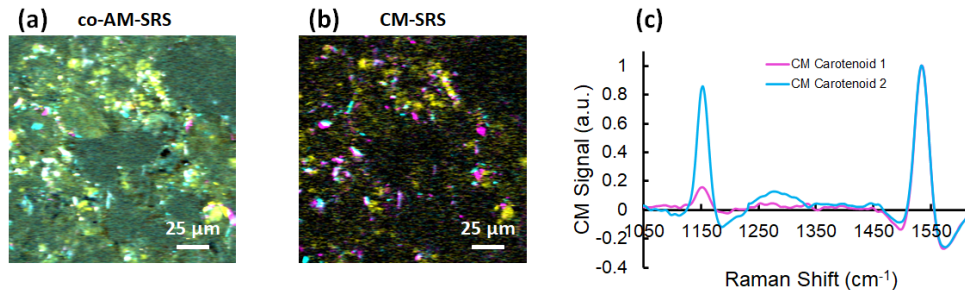


Fig. 4. CM-SRS of sweet potato (a) Co-chirped AM-SRS of sweet potato recorded at three different Raman shifts: 1150 cm^{-1} (cyan), 1520 cm^{-1} (magenta) and 2850 cm^{-1} (yellow). (b) CM-SRS image of sweet potato at the same Raman shifts as the AM-SRS image. (c) Average CM-SRS for all the pixels identified as carotenoid 1 (magenta line) or carotenoid 2 (cyan line). Pixels were identified based on intensity threshold masks. Pixels could only be assigned to one group and were assigned based on spectral similarity.

In our second demonstration of CM-SRS, we imaged an even more heterogeneous colored sample: a pine stem slice. Using AM-SRS, shown in Figs. 5(a)–(c), we recorded high spatial contrast images at Raman shifts of 1362 , 1519 and 1602 cm^{-1} , respectively. Despite the high spatial contrast, the AM-SRS image intensity does not vary with Raman shift. A false-colored RGB merge of Figs. 5(a)–(c), Fig. 5(d), reveals the same spatial intensity distribution as each of its components: AM-SRS offers no chemical contrast in this sample. CM-SRS shows image spatial variation with Raman shift, as seen in Figs. 5(e)–(g). This permitted chemical-specific image segmentation: the segmentation-associated CM-SRS Raman spectra and their deconvolutions are shown in Supplement 1, Figs. S5 and S6. Additionally, we find that the AM-SRS spectra from the same regions are dominated by non-Raman backgrounds, as seen in the AM-SRS spectra Supplement 1, Fig. S7. In Fig. 5(h), we show the resultant RGB merge, demonstrating the highly detailed, chemical-specific imaging capabilities of CM-SRS in complex, heterogeneous, strongly absorbing media.

In many biologically relevant systems, low analyte concentration leads to weak Raman responses, a general challenge to SRS imaging. Here, we demonstrate single cell pharmacokinetics at the few mM level, shown in Fig. 6. Many pharmaceuticals are small molecules used in low concentrations at therapeutic levels. Being small, traditional fluorescence labeling schemes are generally inapplicable. Raman (vibrational) labels, however, can be introduced via chemical substituents with resonances in the cellular “quiet” region [41,42] of the Raman spectrum. Here, we studied real-time single cell pharmacokinetics of HepG2 cells exposed to a small molecule ice recrystallization inhibitor (IRI), Raman-labeled with a cyano group (inset in Fig. 6(c)). Previous work [43] demonstrated that this class of IRIs is effective at the ~ 10 's mM level but can be cytotoxic at higher concentrations. For the IRI used here, we could not resolve an AM-SRS spectrum even at the highest safe concentration. We note that, in this experiment, a high NA illumination objective was required in order to ensure intracellular concentration was measured, as opposed to compound adhered to the cell surface. As is well known, a mismatched NA of the illumination and collection lenses exacerbates XPM background in AM-SRS. In

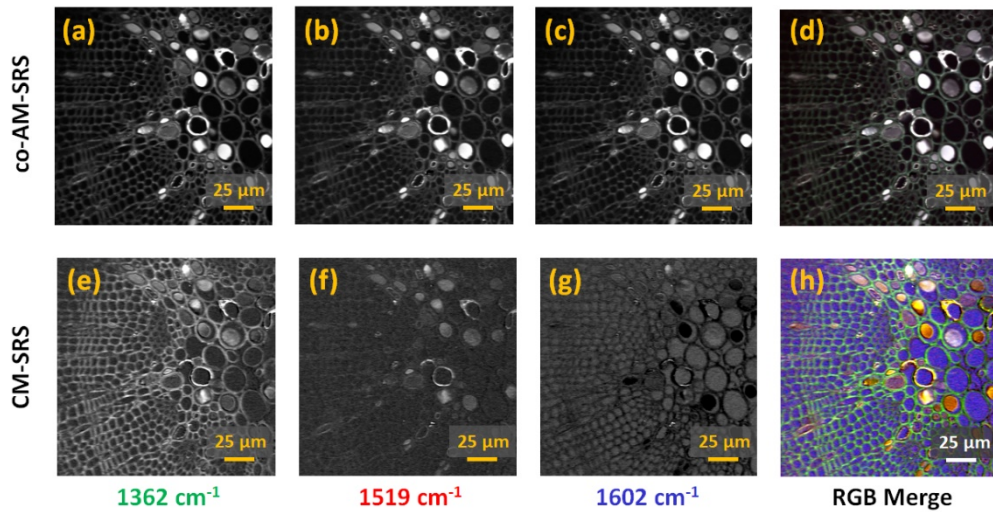


Fig. 5. AM-SRS and CM-SRS of pine stem. (a) AM-SRS of pine stem recorded at 1362 cm^{-1} . (b) AM-SRS of pine stem recorded at 1519 cm^{-1} . (c) AM-SRS of pine stem recorded at 1602 cm^{-1} . (d) RGB merge of (a)-(c) with (a) in green, (b) in red and (c) in blue. The image looks like a grey-scale image because all colors are present with nearly identical intensities in all pixels. (e) CM-SRS of pine stem recorded at 1362 cm^{-1} . (f) CM-SRS of pine stem recorded at 1519 cm^{-1} . (g) CM-SRS of pine stem recorded at 1602 cm^{-1} . (h) RGB merge of (e)-(g) with (e) in green, (f) in red and (g) in blue. In this case, spatial variation is clearly visible.

contrast, CM-SRS revealed a cyano resonance at $\sim 2290\text{ cm}^{-1}$, with no background signals (see [Supplement 1](#), Fig. S8(a)). For kinetics study, HepG2 cells were incubated in a 35 mM solution in cell media and imaged as a function of exposure time. To quantify the pharmacokinetics, the cells were rinsed in fresh media before imaging in order to remove IRI signals from the surrounding media. Initially, no IRI was seen inside the cells. After a few hours' exposure, the drug became confined within the cells. To verify that the drug was uniformly spread within the cells, cell boundaries were imaged at 2850 cm^{-1} (CH-region) using AM-SRS, the drug distribution being measured via CM-SRS at the 2290 cm^{-1} cyano resonance. Images of CH region AM-SRS and cyano CM-SRS, at four hours exposure, are shown in Fig. 6(a) and Fig. 6(b), respectively (for additional representative images of the cyano CM-SRS signals at other time points, see [Supplement 1](#), Fig. S8(b)-(d)). Using CM-SRS, we quantified the pharmacokinetics, shown in Fig. 6(c), of intracellular IRI concentration over 5 hours, whereupon the intra and extracellular concentrations roughly equalized at 35 mM. We anticipate that, as sensitivities continue to improve, CM-SRS may become a useful method for more general label-free, molecule-specific studies of single cell pharmacokinetics.

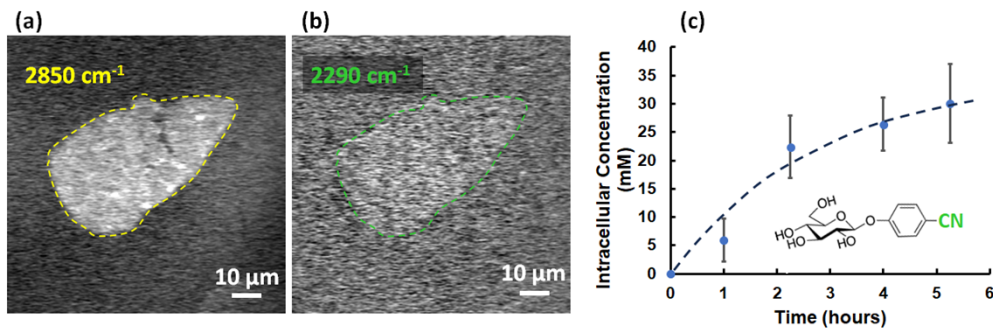


Fig. 6. Pharmacokinetics in living cells. (a) AM-SRS image of HepG2 cells recorded at 2850 cm^{-1} . (b) CM-SRS image of HepG2 cells recorded at 2290 cm^{-1} . This image was recorded 4 hours post IRI exposure and media rinse. (c) Time-dose response of IRI in HepG2 cells. Each data point was measured for at least 3 fields of view. Error bars are the corrected sample standard deviation. Inset: Chemical structure of the IRI used in these experiments.

4. Conclusion

Coherent nonlinear optical processes can be controlled and modulated using techniques which extend beyond the linear optical methods originally developed for radar and subsequently applied to optical spectroscopy and telecommunications. By modulating higher order (i.e. quadratic and above) optical phases with a specific symmetry constraint (maintaining constant intensity), it will be possible to apply nonlinear microscopies to an ever-increasing range of samples and applications areas. We demonstrated here that rapid modulation of exclusively the sign of the quadratic phase can remove background signals in CRM, enabling chemical-specific imaging even in samples where background nonlinear optical processes are strongly dominant. This may become particularly valuable for electronic resonance-enhanced CRM [44–46]. In principle, both FM-SRS (and SR-GOLD) [27] and CM-SRS may be sensitive to frequency-dependent nonlinear background signals near resonances. In CM-SRS, the sum-frequency (i.e. TPA) spectrum is also modulated between broad and narrow bandwidth. Importantly, in CM-SRS, this spectral variation is very narrow, within the laser bandwidths. Since most electronic spectra of condensed phase molecules are broad and featureless, barring the exceptional case of TPA at a sharp origin band, we expect that CM-SRS is relatively immune to such electronic effects. CM-SRS retrieves the chemical identity of the species under study in a background-free manner and opens high-sensitivity, quantitative CRM measurements to new fields of study, including plant biology, material science, mineralogy and others.

Funding. National Research Council of Canada (AI4D-124-1, QSP-052-1); Natural Sciences and Engineering Research Council of Canada (Discovery Grant Program); Canada Foundation for Innovation; Max-Planck-Centre for Extreme and Quantum Photonics.

Acknowledgments. The authors thank Leah McMunn and Prof. Robert Ben (Ottawa) for the HepG2 cells and the IRI compound. We thank Alexander Harper, Siddarth Shivkumar, Leah Frackleton, Mehdi Alizadeh, Dr. Pedram Abdolghader, Dr. Rune Lausten (NRC), Prof. Lora Ramunno (Ottawa), Dr. Andrew Ridsdale (NRC) and Prof. Eric Potma (UC Irvine) for useful discussions.

Disclosures. The authors declare no conflicts of interest.

Data availability. Data underlying the results presented in this paper are not publicly available but will be provided by the authors upon a reasonable request.

Supplemental document. See [Supplement 1](#) for supporting content.

References

1. N. Dudovich, D. Oron, and Y. Silberberg, "Single-pulse coherently controlled nonlinear Raman spectroscopy and microscopy," *Nature* **418**(6897), 512–514 (2002).

2. C. W. Freudiger, W. Min, G. R. Holtom, *et al.*, “Highly specific label-free molecular imaging with spectrally tailored excitation-stimulated Raman scattering (STE-SRS) microscopy,” *Nat. Photonics* **5**(2), 103–109 (2011).
3. T. Ideguchi, S. Holzner, B. Bernhardt, *et al.*, “Coherent Raman spectro-imaging with laser frequency combs,” *Nature* **502**(7471), 355–358 (2013).
4. C. H. Camp Jr and M. T. Cicerone, “Chemically sensitive bioimaging with coherent Raman scattering,” *Nat. Photonics* **9**(5), 295–305 (2015).
5. J.-X. Cheng and X. S. Xie, *Coherent Raman Scattering Microscopy*, 1st ed. (CRC, 2012).
6. J.-X. Cheng and X. S. Xie, “Vibrational spectroscopic imaging of living systems: An emerging platform for biology and medicine,” *Science* **350**(6264), aaa8870 (2015).
7. C. Zhang, D. Zhang, and J.-X. Cheng, “Coherent Raman scattering microscopy in biology and medicine,” *Annu. Rev. Biomed. Eng.* **17**(1), 415–445 (2015).
8. J.-X. Cheng, W. Min, Y. Ozeki, *et al.*, eds., *Stimulated Raman Scattering Microscopy Techniques and Applications*, 1st ed. (Elsevier, 2022).
9. W. Min and X. Gao, “Fundamental detectability of Raman scattering: A unified diagrammatic approach,” *The J. Chem. Phys.* **160**(9), 094110 (2024).
10. Y. Wang, C.-Y. Lin, A. Nikolaenko, *et al.*, “Four-wave mixing microscopy of nanostructures,” *Adv. Opt. Photonics* **3**(1), 1–52 (2011).
11. H. Kim, T. Sheps, P. G. Collins, *et al.*, “Nonlinear optical imaging of individual carbon nanotubes with four-wave-mixing microscopy,” *Nano Lett.* **9**(8), 2991–2995 (2009).
12. M. Andreana, M.-A. Houle, D. J. Moffatt, *et al.*, “Amplitude and polarization modulated hyperspectral stimulated Raman scattering microscopy,” *Opt. Express* **23**(22), 28119–28131 (2015).
13. P. Abdolghader, A. Ridsdale, T. Grammatikopoulos, *et al.*, “Unsupervised hyperspectral stimulated Raman microscopy image enhancement: denoising and segmentation via one-shot deep learning,” *Opt. Express* **29**(21), 34205–34219 (2021).
14. J. C. Mansfield, G. R. Littlejohn, M. P. Seymour, *et al.*, “Label-free chemically specific imaging in planta with stimulated Raman scattering microscopy,” *Anal. Chem.* **85**(10), 5055–5063 (2013).
15. A. Lombardini, A. Lombardini, P. Berto, *et al.*, “Background-suppressed SRS fingerprint imaging with a fully integrated system using a single optical parametric oscillator,” *Opt. Express* **28**(10), 14490–14502 (2020).
16. J. Jiang, D. Grass, Y. Zhou, *et al.*, “Beyond intensity modulation: new approaches to pump-probe microscopy,” *Opt. Lett.* **46**(6), 1474–1477 (2021).
17. H. V. Kastenholz, M. I. Topper, W. S. Warren, *et al.*, “Noninvasive identification of carbon-based black pigments with pump-probe microscopy,” *arXiv*, (2024).
18. M. C. Fischer, J. W. Wilson, F. E. Robles, *et al.*, “Invited Review Article: Pump-probe microscopy,” *Rev. Sci. Instrum.* **87**(3), 031101 (2016).
19. A. F. Pegoraro, D. J. Moffatt, and A. Ridsdale, “Oblique angle transient-reflectivity laser-scanning microscopy for mineral imaging in natural ores,” *Opt. Express* **28**(8), 11946–11955 (2020).
20. K. Kikuchi, “Fundamentals of coherent optical fiber communications,” *J. Lightwave Technol.* **34**(1), 157–179 (2016).
21. J.-M. Liu, “10 - Optical Modulation,” in *Principles of Photonics*, 1st ed. (Cambridge University, 2016), pp. 297–361.
22. X. S. Xie, C. Freudiger, and W. Min, “United States Patent: 8027032 - Microscopy imaging system and method employing stimulated raman spectroscopy as a contrast mechanism,” U.S. patent 8027032 (September 27, 2011).
23. C. W. Freudiger, W. Min, B. G. Saar, *et al.*, “Label-free biomedical imaging with high sensitivity by stimulated Raman scattering microscopy,” *Science* **322**(5909), 1857–1861 (2008).
24. D. Zhang, M. N. Slipchenko, D. E. Leaird, *et al.*, “Spectrally modulated stimulated Raman scattering imaging with an angle-to-wavelength pulse shaper,” *Opt. Express* **21**(11), 13864–13874 (2013).
25. A. H. Hill, E. Munger, A. T. Francis, *et al.*, “Frequency Modulation Stimulated Raman Scattering Microscopy through Polarization Encoding,” *J. Phys. Chem. B* **123**(40), 8397–8404 (2019).
26. S. Heuke and H. Rigneault, “Coherent Stokes Raman scattering microscopy (CSRS),” *Nat. Commun.* **14**(1), 3337 (2023).
27. P. Berto, E. R. Andresen, and H. Rigneault, “Background-Free Stimulated Raman Spectroscopy and Microscopy,” *Phys. Rev. Lett.* **112**(5), 053905 (2014).
28. Y. Silberberg, “Quantum coherent control for nonlinear spectroscopy and microscopy,” *Annu. Rev. Phys. Chem.* **60**(1), 277–292 (2009).
29. D. Meshulach and Y. Silberberg, “Coherent quantum control of two-photon transitions by a femtosecond laser pulse,” *Nature* **396**(6708), 239–242 (1998).
30. T. Hellerer, A. M. K. Enejder, and A. Zumbusch, “Spectral focusing: High spectral resolution spectroscopy with broad-bandwidth laser pulses,” *Appl. Phys. Lett.* **85**(1), 25–27 (2004).
31. A. F. Pegoraro, A. Ridsdale, D. J. Moffatt, *et al.*, “Optimally chirped multimodal CARS microscopy based on a single Ti:sapphire oscillator,” *Opt. Express* **17**(4), 2984–2996 (2009).
32. D. Fu, G. Holtom, C. Freudiger, *et al.*, “Hyperspectral Imaging with Stimulated Raman Scattering by Chirped Femtosecond Lasers,” *J. Phys. Chem. B* **117**(16), 4634–4640 (2013).
33. I. Rocha-Mendoza, W. Langbein, and P. Borri, “Coherent anti-Stokes Raman microspectroscopy using spectral focusing with glass dispersion,” *Appl. Phys. Lett.* **93**(20), 201103 (2008).

34. D. Fu, W. Yang, and X. S. Xie, "Label-free imaging of neurotransmitter acetylcholine at neuromuscular junctions with stimulated Raman scattering," *J. Am. Chem. Soc.* **139**(2), 583–586 (2017).
35. J. Jiang, "Extending the reach and contrast of pump-probe microscopy," Duke University (2020).
36. T. A. Pologruto, B. L. Sabatini, and K. Svoboda, "ScanImage: Flexible software for operating laser scanning microscopes," *BioMed. Eng. OnLine* **2**(1), 13 (2003).
37. M. Mohseni, C. Polzer, and T. Hellerer, "Resolution of spectral focusing in coherent Raman imaging," *Opt. Express* **26**(8), 10230–10241 (2018).
38. J. Cheng, A. Volkmer, L. D. Book, *et al.*, "An epi-detected coherent anti-Stokes Raman scattering (E-CARS) microscope with high spectral resolution and high sensitivity," *J. Phys. Chem. B* **105**(7), 1277–1280 (2001).
39. N. Altangerel, G. O. Ariunbold, C. Gorman, *et al.*, "In vivo diagnostics of early abiotic plant stress response via Raman spectroscopy," *Proc. Natl. Acad. Sci. U.S.A.* **114**(13), 3393–3396 (2017).
40. N. Altangerel, G. O. Ariunbold, C. Gorman, *et al.*, "Reply to Dong and Zhao: Plant stress via Raman spectroscopy," *Proc. Natl. Acad. Sci. U.S.A.* **114**(28), E5488–E5490 (2017).
41. L. Li, H. Wang, and J.-X. Cheng, "Quantitative coherent anti-Stokes Raman scattering imaging of lipid distribution in coexisting domains," *Biophys. J.* **89**(5), 3480–3490 (2005).
42. J. P. Pezacki, J. A. Blake, D. C. Danielson, *et al.*, "Chemical contrast for imaging living systems: molecular vibrations drive CARS microscopy," *Nat. Chem. Biol.* **7**(3), 137–145 (2011).
43. S. Mangan, J. Dagher, V. J. Moulin, *et al.*, "Small molecule ICE recrystallization inhibitors for the cryopreservation of tissue components and tissue constructs," *Cryobiology* **113**, 104615 (2023).
44. L. Wei and W. Min, "Electronic preresonance stimulated Raman scattering microscopy," *J. Phys. Chem. Lett.* **9**(15), 4294–4301 (2018).
45. C. Zong, R. Premasiri, H. Lin, *et al.*, "Plasmon-enhanced stimulated Raman scattering microscopy with single-molecule detection sensitivity," *Nat. Commun.* **10**(1), 5318 (2019).
46. A. J. X. Choorakuttil, A. Pruccoli, M. J. Winterhalder, *et al.*, "Electronically preresonant stimulated Raman scattering microscopy in the visible," *Appl. Phys. Lett.* **123**(16), 163701 (2023).